ISSN (Print) 1226-1750
ISSN (Online) 2233-6656
Journal of Magnetics 28(3), 245-250 (2023) https://doi.org/10.4283/JMAG.2023.28.3.245

Magnetization Dynamics Modeling in a Like Iron-Silicon Thin Film by the Micromagnetic Approach

Messaoud Boufligha[1], Lakhdar Bessissa[2]*, and Djillali Mahi[3]

[1,3]*Electrical Engineering Department, Faculty of Technology, Amar Telidji University, Laghouat, Algeria*
[2]*Materials Science and Informatics Laboratory, University Ziane Achour of Djelfa, Algeria*

(Received 24 October 2022, Received in final form 8 Septembert 2023, Accepted 15 Septembert 2023)

Iron-silicon thin films used as a single layer or in sandwich structures are currently regarded as a promising candidate in high magnetic sensors. A detailed understanding of magnetization dynamics in such thin films is of great interest. In this work, we only focused on modeling the magnetization reversal. Numerical solution to the nonlinear Landau-Lifshitz-Gilbert (LLG) equation can be used to conduct the study. With the help of our developed Matlab code, the simulations were carried out. External field strength, damping parameter and temperature all have an impact on the speed of the magnetization reversal. The validation of our computations is achieved via a separate simulation. It relates to the solution of the standard problem proposed by the micromagnetic Modeling Activity Group (μMAG). The results are in agreement with the ones presented in the National Institute of Standards and Technology (NIST) website.

Keywords : micromagnetic, magnetization reversal, simulation, Fe-Si alloys, damping parameter

1. Introduction

Soft ferromagnetic materials like iron-silicon alloys are effectively used on a large scale in electric motors, generators and transformers. Materials should be scaled down the nano and micro shapes to satisfy some technological requirements [1]. Using advanced fabrication techniques such as sputtering magnetron permit producing iron-silicon (Fe_{100-x}-Si_x) thin films, even with high content of silicon, (x) [2, 3]. These devices are promising in the development of high magnetic sensors and can be used as a single layer or in sandwich structures [4-7]. Magnetization dynamics, often known as the evolution of magnetization is a complicated process that occurs in ferromagnetic materials [8, 9]. The complexity is due to the non linearity and the number of degrees of freedom to be taken into account such as conduction, stress and thermal effects [10-13]. Hence, the main challenge is a deeper understanding of the above process in iron-silicon thin films. It plays a great role in the design of miniaturized ferromagnetic systems and become a current question. It is important to note that the micromagnetism theory is the framework used for studying magnetization phenomena at the microscopic scale. Consequently, the micromagnetic approach is a practical method that can be applied in modelling magnetization dynamics in ferromagnetic materials at nanometer and micrometer scales. It is based on solving numerically the dynamic (LLG) equation.

Previously, many efforts have been concentrated on modelling magnetization dynamics at nano and micro scales in some alloys based on iron. The objective is the study of magnetization reversal and switching processes. Several and specific shapes and geometries of materials are considered [14]. However, modelling magnetization dynamics in iron-silicon nano and micro structures received a little attention. Most authors point on static and equilibrium states computations [15]. Additionally, experimental researchers focus on technical methods of producing iron-silicon thin films and studying several specific phenomena such as ordering [16-20]. Despite, most magnetic properties are identified and explained; the precise knowledge of the physical mechanisms that control the magnetization evolution in iron-silicon thin films is of interest. It helps in the comprehension of phenomena that occurred in magnetic sensors.

In this paper, we are only interested on modelling the magnetization reversal process at zero and finite temper-

*Corresponding author: Tel: +213-660416089
e-mail: lakhdarbessissa@gmail.com

ature in an iron-silicon thin film. The 4 % Si-Fe is used as a reference material. It is well to note that several open and paid micromagnetic tools respectively such as Object Oriented Micromagnetic Frame work (OOMMF) and LLGsimilator are used by the micromagnetic community in numerical computations [21, 22]. In this work, all the simulations were carried out using our developed Matlab code [23]. In this purpose, the (LLG) equation is time-integrated using Runge-Kutta method [24]. In space, it is discretized by the finite difference method.

The validation of our computations is realized by a different simulation [25]. It relates to the solution of the fourth standard problem proposed by (μMAG). In this aim, a rectangular thin film of Permalloy ($Fe_{20}N_{80}$) of size $500\times125\times3$ nm^3 is taken into consideration.

The structure of the current work is as follows: after the introduction in section 1, some details about the used micromagnetic approach and simulation details are presented in section 2. Results, discussion, the validation and the confirmation of the findings are summarized in section 3. The paper is closed with conclusions.

2. Modeling and Simulation Details

It is well known that with the theory of micromagnetism one can study the magnetization dynamics processes. This theory allows evaluating the total magnetic free energy, E_{tot}, witch is the sum of four terms.

$$E_{tot} = E_{exch} + E_{anis} + E_{dem} + E_{ext} \tag{1}$$

Where :

- E_{exch} is exchange energy: It is related to the formation of the domain wall,
- E_{anis} is magnetocristalline energy: It is closely associated with the crystallographic directions along which the magnetic moments are aligned,
- E_{dem} is magnetostatic energy: It originates from the long-range dipole-dipole interactions,
- E_{ext} is the energy due to an external field: It forces the magnetization to become oriented in the applied field directions.

The analysis of the magnetization dynamics processes in ferromagnetic thin films is based on the solution of the *(LLG)* equation defined by:

$$\frac{dM}{dt} = -\frac{\gamma}{1+\alpha^2}(M\times H_{eff}) - \frac{\gamma\alpha}{\left(1+\alpha^2\right)M_s} M\times\left(M\times H_{eff}\right) \tag{2}$$

Where :

- M is the magnetic moment per unit volume,
- γ corresponds to the gyromagnetic ratio,
- α denotes the damping parameter,
- M_s is the saturation magnetization,
- H_{eff} is the total effective field: It is the variation of the total free energy with respect to the magnetization and is given by:

$$H_{eff} = -\frac{1}{\mu_0}\frac{\delta E_{tot}}{\delta M} \tag{3}$$

Where μ_0 being the magnetic permeability of the vacuum.

When analyzing time-dependent magnetization processes at finite temperature, a thermal field H_{therm} is added to the effective field, it is given by:

$$H_{therm} = G\sqrt{\frac{2\,k_b T\,\alpha}{\mu_0\,\gamma V\,M_s dt}} \tag{4}$$

Where :

- dt is the simulation time-step,
- K_b is the Boltzmann constant,
- T is the temperature of the sample,
- V is the volume of the computational cell, and
- G is a random three-dimensional vector.

Including the thermal field leads to the stochastic form of the (LLG) equation. This thermal field accounts for the interactions of the magnetization with the microscopic degrees of freedom which cause fluctuations of the magnetization distribution. It satisfies the following statistical properties.

$$\left\langle H_{therm}(t)\right\rangle = 0 \tag{5}$$

$$\left\langle H_{thermi}(t) H_{therm\,j}(t')\right\rangle = 2D\delta_{ij}\;\delta(t-t') \tag{6}$$

Where, i and j represent the Cartesian indices. The Kronecker δ_{ij} expresses the fact that the different components of the thermal field are uncorrelated. The Dirac function shows that the autocorrelation time of the thermal field is much shorter than the response time of the system.

The micromagnetic equation can be numerically discretized in space by using the finite difference method, where the sample is divided into regular cells, or the finite element method, where the cell can take any shape. In the absence of the surface anisotropy, the discretization is enforced by the Neumann boundary conditions expressed as:

$$\frac{\partial m}{\partial n} = 0 \tag{7}$$

Where $m=M/M_s$ is the dimensionless magnetization and n is the outer unit normal of the surface. The sample proposed is a square thin film of size $L_x \times L_y \times L_z$ where L_x=120 nm, L_y=120 nm, L_z=3 nm as showed by Fig. 1.

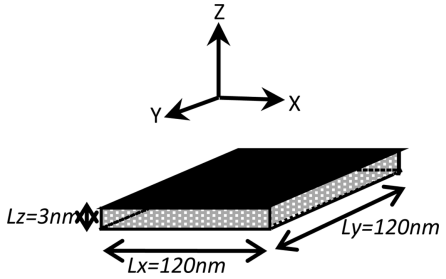

Fig. 1. Geometry of the proposed thin film.

The thin film is discretized into $N_x \times N_y \times N_z$ cells where N_x, N_y, and N_z respectively represent the number of cells along the x, y and z axis. A single cell is taken into consideration along the z-axis, it leads to a pseudo two-dimensional grid of cells. The initial magnetization, $M_{initial}$ is chosen oriented along the positive x-axis. Cartesian coordinates are used. The moment within one cell can be expressed as:

$$M = M_s\left(m_x,\ m_y,\ m_z\right) \tag{8}$$

Where m_x, m_y, m_z are respectively the dimensionless components of the magnetization in the direction of x-axis, y-axis and the z-axis. The three-dimensional moments are positioned at the centers of the cells.

The Eq. (2) used in the simulation can be rewritten in the dimensionless form as follows:

$$\frac{dm}{d\tau} = -\frac{\gamma}{1+\alpha^2}(m \times h_{eff}) - \frac{\gamma\alpha}{1+\alpha^2} m \times (m \times h_{eff}) \tag{9}$$

Where τ and $h_{eff} = H_{eff}/M_s$, represent respectively the dimensionless time-step and the normalized total effective field.

The micromagnetic calculations start with the evaluation of the components of the total effective field. The computations of the external, anisotropic and the exchange components are easily done. The difficulty lies in computing the demagnetizing field contribution; as a result, advanced methods are used. In this work, the demagnetizing field calculation is based on the three-dimensional dipolar approximation [26]. Thus, the demagnetizing field results in a convolution product between the magnetization M and the demagnetizing tensor T_{dem}. So, the components of this contribution can be computed by a direct product using the direct and inverse Fourier transforms as follows:

$$H_{dem} = TF^{-1}\left(TF\left(T_{dem}\right).TF\left(M\right)\right) \tag{10}$$

The evaluation of H_{therm} is performed by the computation of the components of the vector, G. These components are random numbers having uniform distribution generated with an updated seed and converted into a Gaussian distribution using the Box-Muller transform.

It is worth noting that alloying iron material with silicon leads to a destroy of the crystal symmetry, so to a decrease of the magnetocrystalline anisotropy. Consequently, the first order anisotropy constant, K_1 can be only taken into account such as in our reference material. It is showed that the intrinsic parameters in iron-silicon alloys such as, the anisotropy constant K_1 and the saturation magnetization M_s are function of percentage of the silicon in iron, (p_{si}). These results are presented in [27, 28]. They are approximated by the polynomial interpolations of the measurements as reported in [29] and defined by:

$$K_1\left(p_{si}\right) = -4333\,p_{si} + 480 \ \ [\mathrm{ker\,g/cm^3}] \tag{11}$$

$$M_s\left(p_{si}\right) = 4p_{si}^3 - 82p_{si}^2 - 206\,p_{si} + 21580 \ \ [G] \tag{12}$$

Where 1 erg/cm^3 = 0.1 J/m^3 and 1G = (1000/4π) A/m.

In this context, the material parameters used in our numerical simulations are: the magnetocrystalline anisotropy constant, $K_1 = 3.1 \times 10^4$ J/m^3, the saturation magnetization $M_s = 1.71 \times 10^6$ A/m and the exchange constant, $A = 1.7 \times 10^{-11}$ J/m, which is an approximated value existing in the literature. The gyromanetic ratio, γ is set equal to 2.211×10^5 m/(As), while the damping parameter can take various values in our simulations. Knowing the following dimensionless components of the total effective field, h_{effx}, h_{effy} and h_{effz}, we start integrating the dynamic equation using the fourth order Runge-Kutta method. The time evolution of the magnetization is computed.

3. Results and Discussion

In this section, we begin by analyzing the effect of the strength of the applied field on the reversal magnetization process at zero temperature. The initial magnetization was aligned along the positive x-axis. The spatial discretization of (40×40×1) cells of size 3×3×3 nm^3 is chosen. It is in the order of the exchange length. The damping parameter, α=0.0065. Figure 2 shows the time evolution of the average dimensionless component of magnetization, $\langle m_x \rangle$ in the thin film subjected to different values of the field strength, applied in the opposite x-direction.

As observed, the speed of the magnetization reversal depends on the strength of the applied field. To understand the inversion process, the result displayed by Fig. 3 which represents a distribution of spins when $\langle m_x \rangle$ first crosses zeros is inevitable. It is obtained in the case of a field strength, H=100 kA/m and a damping parameter, α =0.0065. It can be seen a structure governed by the

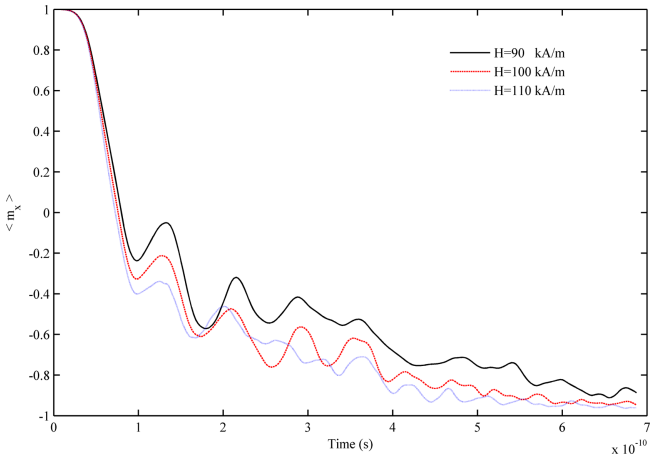

Fig. 2. (Color online) Time evolution of the average dimensionless component of the magnetization, $<m_x>$ during the reversal process in the iron-silicon thin film for different field strengths, with the damping parameter, α=0.0065 computed using a spatial discretization of (40×40×1) cells.

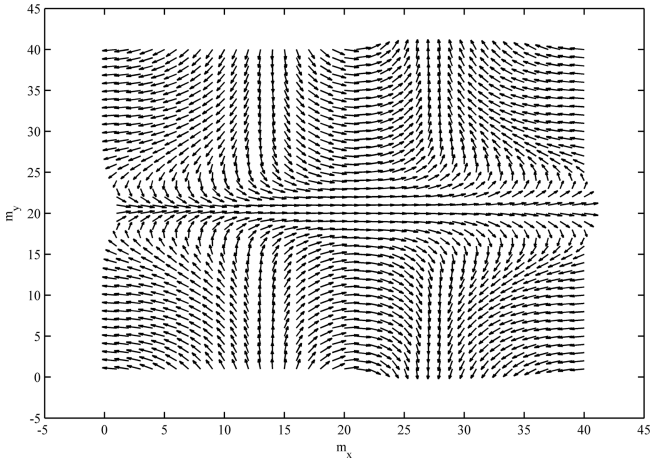

Fig. 3. Distribution of spins in the iron-silicon thin film when $<m_x>$ first crosses zero in the case of field strength, H=100 kA/m with damping parameter, α=0.0065 computed using a spatial discretization of (40×40×1) cells.

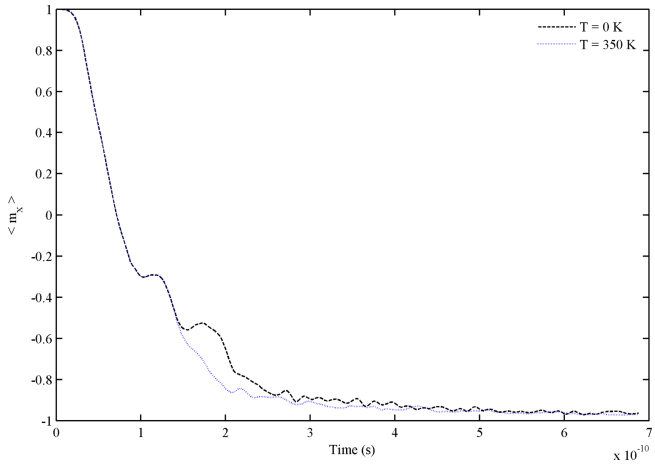

Fig. 4. (Color online) Time evolution of the average dimensionless component of the magnetization, $<m_x>$ during the reversal process in the iron-silicon thin film for different values of temperature with damping parameter α=0.0065, computed using a spatial discretization of (40×40×1) cells.

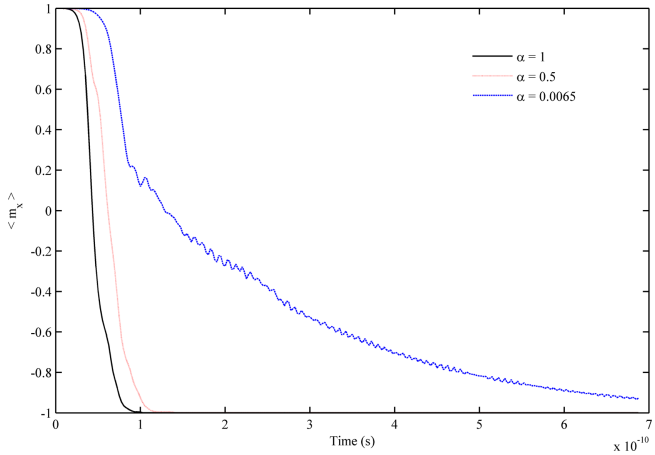

Fig. 5. (Color online) Time evolution of the average dimensionless component of the magnetization, $<m_x>$ during the reversal process in the iron-silicon thin film for different values of damping parameter with a strength field of H=1400 kA/m, computed using a spatial discretization of (40×40×1) cells.

rotation of spins during the reversal process. It is in agreement with the domain theory.

Now, we tried to include thermal effects. An external field of 150 kA/m is applied in the thin film plane in the opposite direction of the x-axis. The value of the damping parameter α=0.0065. Figure 4 shows the time evolution of the average dimensionless component of magnetization, $<m_x>$, for the values of temperature, T=0 K and T=350 K.

As noted, the speed of the magnetization reversal is slightly affected when the temperature of the thin film is increased. Including thermal fluctuations allows magnetization to rotate out of its preferred orientation [30].

Another parameter that can affect the magnetization reversal mechanism is the damping parameter. Figure 5 shows the time evolution of the average dimensionless component of magnetization, $<m_x>$ in the thin film subjected to field strength of 1400 kA/m. The later is applied in the thin film plane in the opposite direction of the x-axis for different values of the damping parameter.

It can be seen that the speed of the magnetization reversal decrease for low damping value and increase for high value.

In the following of this part, we are interested to the

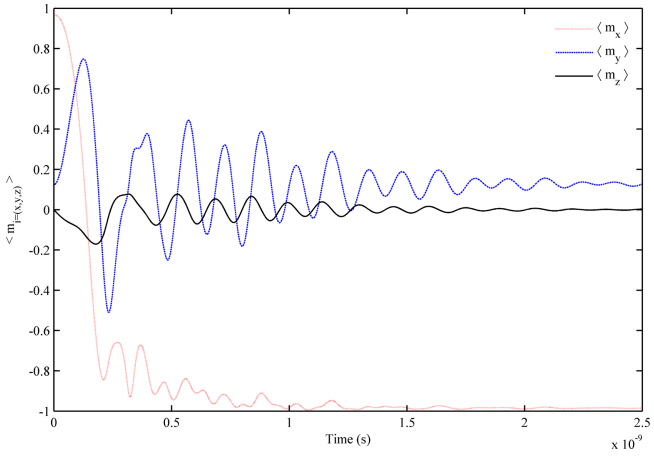

Fig. 6. (Color online) Time evolution of the average dimensionless components of the magnetization $<m_{i=(x,y,z)}>$ during the reversal process by the first field in the Permalloy thin film, computed using a spatial discretization of 128×32×1 cells.

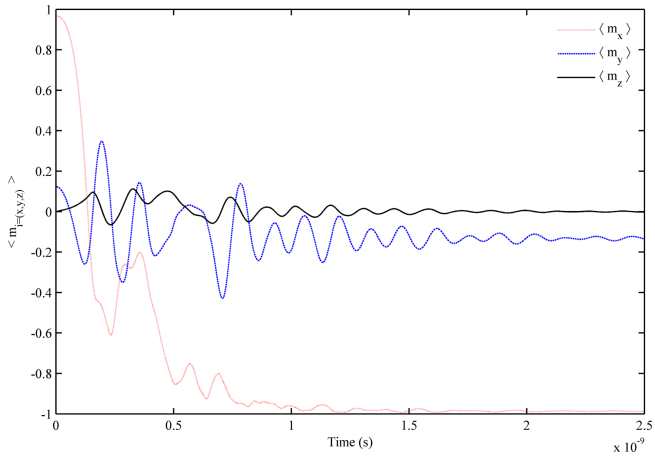

Fig. 7. (Color online) Time evolution of the average dimensionless components of the magnetization $<m_{i=(x,y,z)}>$ during the reversal process by the second field in the Permalloy thin film, computed using a spatial discretization of 128×32×1 cells.

validation of our computations. It is worth to note that in thin films, a specific uniaxial anisotropy is induced by applying an external magnetic field during the fabrication process. Constant, K_u is used for the identification of the this kind of anisotropy. When alloying Iron with Nickel, the above constant reached the value zero in the case of the Permalloy ($Fe_{20}N_{80}$) used in the validation, therefore, $K_u = 0$ J/m^3. Others typical parameters for this material are: the exchange constant, $A = 1.3\times10^{-11}$ J/m, the saturation magnetization, $M_s = 8.0\times10^5$ A/m. and the damping constant, $\alpha = 0.02$. The gyromanetic ratio, $\gamma = 2.211\times10^5$ m/(As). We performed the simulations using the spatial discretization of (128×32×1) cells of size 3.90625×3.90625×3 nm^3. A stopping criterion is added with the maximum number of iterations. The variation of magnetization is evaluated and compared approximately to the values existing in the range of $max\left|\frac{1}{M_s}\frac{dM}{dt}\right| \le 0.01\frac{rd}{ns}$. In order to obtain the static equilibrium (S-state), a saturating field is applied along the (1,1,1) direction, this field is deacreased slowly to zero and leaving the system relaxing. The (S-state) is regarded as the recent initial state and the magnetization is reversed by two fields applied separately in the (x-y) plane of the thin film. The components of the first field applied and directed 170° counter-clockwise from the positive x-axis are: $\mu_0 H_{1x} = -24.6$ mT, $\mu H_{1y} = 4.3$ mT, $\mu_0 H_{1z} = 0$ mT. The components of the second field applied and oriented 190° counter-clockwise from the positive x-axis are: $\mu_0 H_{2x} = -35.5$ mT, $\mu_0 H_{2y} = -6.3$ mT, $\mu_0 H_{2z} = 0$ mT. Figure 6 shows the time evolution of the average dimensionless components of magnetization, $<m_x>$, $<m_y>$ and $<m_z>$ when the first field is applied. Similarly, Fig. 7 shows the time evolution of the average dimensionless components of magnetization of the aforementioned components when the second field is applied.

It can be observed that the last two plots are in agreement with the results submitted to (mumag) website. A rigorous confirmation of this is done by a simulation for 1 ns (10^{-9} s) to obtain the time evolution of the average dimensionless component of magnetization, $<m_y>$ respectively to the inversion process by the first and the second fields.

It can be observed that in the case of the inversion by

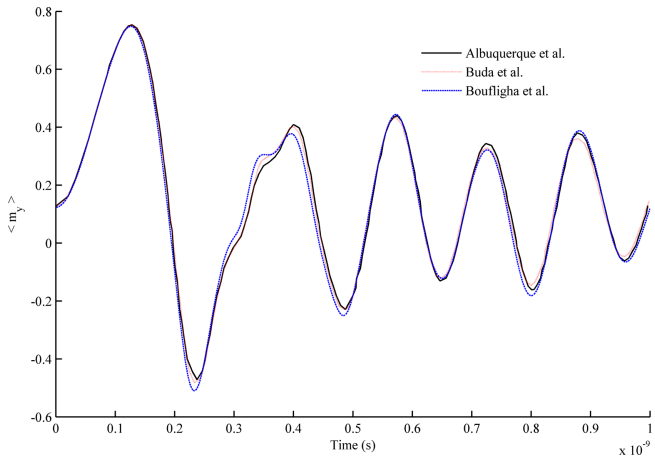

Fig. 8. (Color online) Comparison of the time evolution of the average dimensionless component of magnetization, $<m_y>$ in the Permalloy thin film obtained by our code with some reference plots presented in (mumag website) in the case of the inversion by the first field.

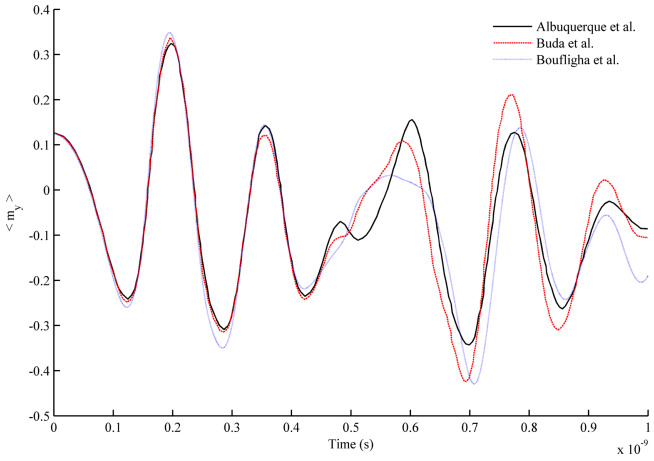

Fig. 9. (Color online) Comparison of the time evolution of the average dimensionless component of the magnetization, $<m_y>$ in the Permalloy thin film obtained by our code with some reference plots presented in (mumag website) in the case of the inversion by the second field.

the first field our solution match slightly the reference plots as showed by Fig. 8. Concerning the inversion by the second field, as displayed by Fig. 9, our result is also agree with the proposed solutions, but we noted that all the solutions available in the above website disagree after a certain time. The discrepancies can be related to the high sensitivity of the micromagnetic dynamic simulations, the use of various algorithms in computing demagnetizing field, time integrating schemes and the chosen spatial discretization.

4. Conclusions

Magnetization dynamics at zero and finite temperature in a like iron-silicon thin film is analyzed. We are concentrated on modeling the reversal magnetization process. Simulations are realized by our developed Matlab code based on solving the (LLG) equation in their deterministic and stochastic forms. The speed of the magnetization reversal is affected by the strength of the applied field, the temperature and the damping parameter. The standard problem proposed by (μMAG) is used to achieve the validation of our simulations. The results provided by the solution of the above problem are confirmed by a comparison with the ones presented in (mumag) website. The flexibility of the at home code to a study involving electrodynamics phenomenon is allowed.

References

[1] V. P. Elanjeitsnni, K. S. Vadivu, and B. M. Prasanth, Mater. Res. Express 9 (2022).
[2] X. N. Li, S. B. Li, L. F. Nie, H. Li, C. Dong, and X. J. Jang, Thin Solid Films **518**, 7390 (2010).
[3] K. Wasa, M. Kitabatake, and H. Adachi, Thin Film Materials Technology, Springer (2004).
[4] O. Gaoyuan, C. Xi, L. Yongfeng, M. Chad, and C. Jun, J. Magn. Magn. Mater. **481**, 234 (2019).
[5] Y. Ercüment and D.Y. Gizem, (CSJ) **38**, 285 (2017).
[6] P. Jantaratana and C. Sirisathitkul, J. Magn. Magn. Mater. **281**, 399 (2004).
[7] M. Phan and H. Peng, Progress in Materials Science **53**, 323 (2008).
[8] A. Barman, S. Mondal, S. Sahoo, and A. De, J. Appl. Phys. 128 (2020).
[9] G. Bertotti, I. D. Mayergoyz, and C. Serpic, Nonlinear Magnetization Dynamics in Nanosystems, Springer, Oxford (2009).
[10] S. Couture, R. Chang, I. Volvach, A. Goncharov, and V. Lomakin, IEEE **53**, 12 (2017).
[11] B. Zhu, C. C. H. Lo, S. J. Lee, and D. C. Jiles, J. Appl. Physics **89**, 7009 (2001).
[12] P. A. Voltairas, D. I. Fotiadis, and C. V. Massalas, IJES **38**, 903 (2000).
[13] D. V. Bercov, Handbook of Magnetism and Advanced Magnetic Materials (2007).
[14] J. Fidler, T. Schrefl, V. D. Tsiantos, W. Scoltz, and D. Suess, Computational Materials Science **24**, 554 (2002).
[15] A. S. Quondam and M. Pompei, (RTSI), IEEE 226 (2015).
[16] R. Nouar, Thesis, University of Belfort-Montbeliard (2009).
[17] M. Kotb, A. H. Saudy, S. Hassballa, and M. M. Eloker, Modern Trends in Physics Research **86**, 82 (2013).
[18] J. M. Ting, and S. W. Hung, Diamond and Related Materials **15**, 1834 (2006).
[19] T. Meydam, H. Kockar, and P. I. Williams, J. Magn. Magn. Mater. **254**, 91 (2003).
[20] F. Gonzalez and Y. Houbaert, Revista de Metalurgia. **49**, 178 (2013).
[21] M. J. Donahue, OOMMF User's guide, 1.1b0, (2000).
[22] M. R. Scheinfein and E. A. Price, LLGMicromagnetic Simulaor Manual v.01 (2015).
[23] R. H. Brian, L. L. Ronald, and M. R. Jonathan, A guide to Matlab for Beguinners and Experienced Users (2001).
[24] M. Boufligha, AMSE Journals, Advances D **21**, 1 (2016).
[25] A. Romeo, G. Finocchio, M. Carpentieri, L. Torres, B. Consolo, and A. Azzerboni, Physica B **403**, 464 (2008).
[26] Y. Nakatani, Y. Uesaka, and N. Hayachi, J. Appl. Phys. **28**, 2485 (1989).
[27] D. Jiles, Introduction to Magnetism and Magnetic Materials (2015) p. 455.
[28] F. Fiorillo, Measurements and Characterization of Magnetic Materials (2004) p. 39.
[29] R. M. Bozorth, Ferromagnetism, IEEE press 1993.
[30] V. Tsiantos, W. Scholz, D. Suess, T. Schrefl, and J. Fidler, J. Magn. Magn. Mater. **242**, 999 (2002).